Astron. Astrophys. 347, 321–334 (1999)

ASTRONOMY AND ASTROPHYSICS

Oscillations in a magnetic solar model

I. Parallel propagation in a chromospheric and coronal magnetic field with constant Alfvén speed

Balázs Pintér and Marcel Goossens

Centrum voor Plasma Astrofysica, K.U. Leuven, Celestijnenlaan 200 B, B-3001 Heverlee, Belgium

Received 24 November 1998 / Accepted 29 April 1999

Abstract. Oscillation eigenmodes are studied for a planar solar model with a non-uniform horizontal magnetic field in the atmosphere. The three layer atmospheric model is the same as in Tirry et al. (1998). The analysis in that paper is extended to a wide range of parameters.

Different types of oscillation modes are determined for a wide range of the magnetic field strength and for different degrees of the spherical harmonic. The emphasis is on the possible coupling of global solar oscillation modes to localized continuum eigenmodes of the magnetic atmosphere. For propagation parallel to the magnetic field, the global oscillation modes can couple only to slow continuum modes and this is found to occur for a rather large range of parameters.

In addition to the damping of global oscillation modes due to resonant absorption it was found that the interaction of global eigenmodes with slow continuum modes leads to unanticipated behaviour of global eigenmodes. The rather strange behaviour in the slow continuum involves the disappearance and appearance of global modes and splitting and merging of global modes.

Additionally, frequency shifts of global modes due to the magnetic field have been examined. The shifts are compared to observations.

Key words: Magnetohydrodynamics (MHD) – Sun: magnetic fields – Sun: oscillations

1. Introduction

The sun exhibits a large number of globally coherent oscillations with frequencies of some mHz. These acoustic oscillations are generated deeply inside the sun. They propagate towards the solar surface, and become evanescent in the atmosphere.

Observations reveal that the frequency shifts have a periodicity of eleven year, in parallel with the solar cycle. Attempts have been made to identify the changes in the solar structure that can cause the measured frequency shifts during the solar cycle.

Libbrecht & Woodard (1990) have shown that the measured frequency shifts depend strongly on the frequency and weakly on the degree of the spherical harmonic for low- and intermediate-l modes.

Campbell & Roberts (1989) were the first to study the effects of a chromospheric magnetic field on the global oscillations of the sun. They considered a plane stratified polytrope in the solar interior with an overlying isothermal atmosphere which is embedded in a horizontal magnetic field of constant Alfvén speed. Evans & Roberts (1990) removed the assumption of a constant Alfvén speed and considered instead a constant chromospheric magnetic field. These papers consider propagations parallel to the equilibrium magnetic field. Jain & Roberts (1994) studied modes propagating obliquely to the magnetic field.

Tirry et al. (1998) have taken into account the possibility of resonant coupling of global magnetoacoustic modes to localized magnetohydrodynamic (MHD) waves. The principal goal of Tirry et al. (1998) was to show that global acoustic solar oscillations can couple to resonant waves and that this resonant coupling causes the global oscillation modes to be damped. Tirry et al. (1998) considered only a small portion of the relevant parameter space as far as magnetic field strength and the degree l of the spherical harmonic are concerned. They took $\beta = 0.2$ (corresponding to a magnetic field of $B \approx 440\,\mathrm{G}$ at the base of the magnetic atmosphere) and $l = 100$.

The present study extends the investigation of Tirry et al. (1998) to a far wider range of parameters. Special attention is paid to the effect of the coupling between the global and local modes. This coupling changes eigenmodes to quasimodes with complex frequencies. The interaction of global oscillation modes with localized slow continuum modes results in several new phenomena of which the splitting of one oscillation mode into two modes, the merging of two oscillation modes into a single mode and the existence of several interacting modes are surprising examples.

Internal gravity modes have also been found, which oscillate in the transition layer.

The width of the transition layer and the ratio of the coronal and photospheric temperature are fixed. Effects due to variations in the temperature profile are investigated in Vanlommel & Čadež (1998). Sect. 2 presents the equilibrium model and describes the procedure for solving the eigenvalue problem. The results are collected in two sections. Sect. 3 deals with global so-

Send offprint requests to: M. Goossens

lar eigenmodes in a field free medium. In Sect. 4, we study the magnetic effects on global oscillation eigenmodes, that propagate parallel to the magnetic field lines. The discussion and conclusions are given in Sect. 5.

2. Model

This paper follows the analysis of Tirry et al. (1998). The reader is referred to this paper for the details of the derivation of the dispersion relation. We briefly summarize the equations for the static equilibrium model and for the linear oscillations.

The solar model used in Tirry et al. (1998) and in the present paper consists of three plane parallel horizontal layers. The plasma is vertically stratified by a constant gravitational acceleration, $\mathbf{g} = g\mathbf{e}_z$, in a system of Cartesian coordinates with the z-axis positively oriented towards to the solar centre. In the basic state, the physical quantities (the equilibrium density ρ_0, gas pressure p_0, temperature T_0 and magnetic induction $\mathbf{B}_0$) are inhomogeneous in the z direction. The plasma obeys the perfect gas law, and it is initially in magnetohydrostatic equilibrium.

The square of the characteristic speeds (sound speed, Alfvén speed and cusp speed, respectively) are defined as

$$v_s^2(z) \equiv \gamma \frac{\mathcal{R}}{\mathcal{M}} T_0(z), \;\; v_A^2(z) \equiv \frac{B_0^2(z)}{\mu_0 \rho_0(z)}, \\ v_c^2(z) \equiv \frac{v_A^2(z) v_s^2(z)}{v_A^2(z) + v_s^2(z)}, \tag{1}$$

where γ is the ratio of specific heats, $\mathcal{R} = 8.3\ 10^3$ g mol^{-1} m^{2}s^{-2} K^{-1} is the universal gas constant, $\mathcal{M}$ is the mean molar mass for a fully ionized hydrogen plasma.

The region $z > 0$ represents the **solar interior** (convection zone and the overlying photosphere). We assume that the gas is polytropic there:

$$p_0^m(z) \sim \rho_0^{1+m}(z), \tag{2}$$

where m is the polytropic index. In this region the magnetic field is neglected. The region is adiabatically stratified in order to be in convective equilibrium (no buoyancy is allowed): $m = \frac{1}{\gamma - 1}$. The temperature decreases linearly until it reaches its minimum at $z = 0$.

The **transition layer** covers basically the solar chromosphere. In this intermediate region, the temperature increases linearly from its minimal value $T_p \equiv T_0(z{=}0)$ to its maximum $T_c \equiv T_0(z{=}{-}L)$ going from the top of the convection zone to the overlying atmosphere.

The overlying atmosphere represents the **corona** assumed to be isothermal.

Above the convection zone the magnetic flux tubes are spread out and fill the atmosphere as a magnetic canopy. For that reason the transition layer and the corona are assumed to be embedded in a horizontal magnetic field. The coordinate system is chosen in such a way that the magnetic field lines are parallel to the x axis: $\mathbf{B}_0(z) = B_0(z)\mathbf{e}_x$. We assume that the plasma-β, the ratio of the gas pressure to the magnetic pressure $\left(\frac{p(z)}{B^2(z)/2\mu}\right)$, is constant.

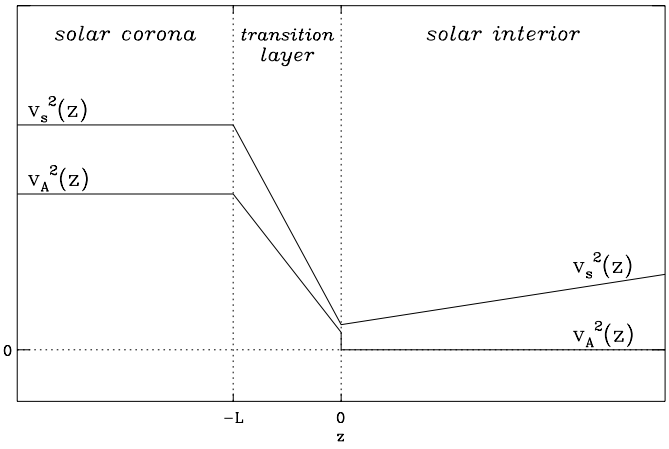

Fig. 1. The schematic profile of the sound speed and the Alfvén speed in the three layer model. The positive z-direction points towards the solar centre.

The squares of the sound speed and of the Alfvén speed are:

$$v_s^2(z) = \begin{cases} \gamma \frac{\mathcal{R}}{\mathcal{M}} T_c, & z \leq \text{-}L, \\ \gamma \frac{\mathcal{R}}{\mathcal{M}} T_p (1 + \alpha_0 z), & \text{-}L \leq z \leq 0, \\ \gamma \frac{\mathcal{R}}{\mathcal{M}} T_p (1 + \frac{z}{z_0}), & z \geq 0. \end{cases}$$

$$v_A^2(z) = \begin{cases} \frac{2}{\gamma \beta} v_s^2(z), & z \leq 0, \\ 0, & z > 0. \end{cases}$$

Here T_p and T_c are the minimal value and the coronal value of the temperature, respectively. In order to model an adiabatically stratified solar interior, $z_0 \equiv (1 + m)H_0$, with $H_0 \equiv \frac{\mathcal{R} T_p}{g \mathcal{M}}$, known as the isothermal pressure scale height at $z = 0$. The relative temperature variation in the transition layer is $\alpha_0 \equiv -\frac{T_c - T_p}{L T_p}$. Note that z_0 is positive while α_0 is negative.

The linear oscillations are described by the linearized MHD equations. Ohmic heating is included via resistivity. Other dissipative effects, such as thermal conductivity and viscosity are ignored. The perturbed quantities are Fourier analyzed with respect to the ignorable horizontal coordinates x and y and put proportional to $\exp(ik_x x{+}ik_y y)$ with k_x and k_y the components of the horizontal wave vector. In a normal mode analysis the time dependence is prescribed by the factor $\exp(-i\omega t)$ where ω is the eigenfrequency that has to be determined. The perturbed quantities then take the form:

$$f_1(x, y, z, t) = f(z; \omega, k_x, k_y) e^{i(k_x x + k_y y - \omega t)}. \tag{3}$$

Dissipation can be ignored with the exception of localized domains where steep gradients occur. In these dissipative regions, the dissipative MHD equations are required for a physically meaningful description of the MHD waves while ideal MHD gives an accurate description of the wave dynamics elsewhere.

The set of linearized ideal MHD equations, can be reduced to two ordinary differential equations of the first order for the vertical component of the Lagrangian displacement $\xi_z(\equiv -i\omega v_z)$ and for the Eulerian perturbation of the total (magnetic and thermal) pressure:

$$D(z)\frac{d\xi_z(z)}{dz} = C_1(z)\xi_z(z) - C_2(z)P(z),$$
$$D(z)\frac{dP(z)}{dz} = C_3(z)\xi_z(z) - C_1(z)P(z). \tag{4}$$

The coefficient functions D, C_1, C_2 and C_3 are

$$D(z) = \rho_0(v_s^2(z)+v_A^2(z))(\omega^2-\omega_c^2(z))(\omega^2-\omega_A^2(z)),$$
$$C_1(z) = -g\rho_0(z)\omega^2(\omega^2-\omega_A^2(z)),$$
$$C_2(z) = (\omega^2-\omega_A^2(z))(\omega^2-\omega_s^2(z)) - \omega^2k_y^2v_A^2(z) \tag{5}$$
$$C_3(z) = \left[\rho_0(z)(\omega^2-\omega_A^2(z)) - g\frac{d\rho_0(z)}{dz}\right]D(z) + g^2\rho_0^2(z)(\omega^2-\omega_A^2(z))^2$$

Here ω_s, ω_A and ω_c are the local sound frequency, the local Alfvén frequency and the local cusp frequency. Their squares are given by

$$\omega_s^2(z) = v_s^2(z)(k_x^2+k_y^2), \quad \omega_A^2(z) = v_A^2(z)k_x^2,$$
$$\omega_c^2(z) = v_c^2(z)k_x^2. \tag{6}$$

In the case of parallel propagation ($k_y = 0$), the coefficient functions reduce to

$$D(z) = \rho_0(v_s^2(z)+v_A^2(z))(\omega^2-\omega_c^2(z)),$$
$$C_1(z) = -g\rho_0(z)\omega^2,$$
$$C_2(z) = (\omega^2-\omega_s^2(z)) \tag{7}$$
$$C_3(z) = \left[\rho_0(z)(\omega^2-\omega_A^2(z)) - g\frac{d\rho_0(z)}{dz}\right]D(z) + g^2\rho_0^2(z)(\omega^2-\omega_A^2(z))$$

Eqs. (4) govern the linear motions of a one-dimensionally stratified magnetic plasma in a gravitational field. When these equations are supplemented with boundary conditions they define an eigenvalue problem for ω.

Eqs. (4) in their general form, with the coefficient function $D(z)$ given in Eq. (5), are singular at the locations $z = z_A$ and $z = z_c$ where either of the two conditions

$$\omega = \omega_A(z_A) \quad \text{or} \quad \omega = \omega_c(z_c) \tag{8}$$

for the Alfvén resonance or for the slow resonance is satisfied.

The frequency matching (8) indicates a resonant wave transformation due to the excitation of a local Alfvén continuum mode at $z = z_A$ or a slow continuum mode at $z = z_c$.

In case of propagation parallel to the magnetic field lines, there is no Alfvén resonance and only the slow resonance survives as can be seen from the simplified version of D. Global oscillations that propagate parallel to **B** can only interact resonantly with local slow continuum modes.

In order to remove the singularities from the mathematical analysis, dissipation has to be included within a comparatively thin layer around the position where the resonant condition (8) is satisfied. The thickness of the dissipative layer is a function of the dissipation rate and the local profile of the cusp frequency or Alfvén frequency. For more details see Tirry & Goossens (1996).

Dissipation damps the eigenmodes and the eigenfrequency becomes complex: $\omega = \omega_r + i\omega_i$ where $\omega_r \gg |\omega_i|$. In this case, the resonances occur when the real part of the eigenfrequency satisfies the conditions (8): $\omega_r = \omega_A(z_A)$ or $\omega_r = \omega_c(z_c)$.

Analytical solutions can be found for $\xi_z(z)$ and $P(z)$ in the solar interior ($z \geq 0$) and in the corona ($z \leq -L$). However, Eqs. (4) have to be integrated numerically in the transition layer, $-L \leq z \leq 0$.

The dispersion relation is obtained from the continuity conditions for the Lagrangian perturbation of the displacement and of the total pressure, ξ_z and $P+\rho_0 g\xi_z$, at the boundaries of the transition layer ($z = 0$ and $z = -L$).

In addition, we require that the perturbation of the kinetic energy density,

$$E_{kin}(z) \equiv \frac{1}{2}\rho_0(z)\omega^2|\boldsymbol{\xi}(z)|^2, \tag{9}$$

vanishes as $z \to \pm\infty$. This condition means that the analysis is restricted to non-leaky eigenmodes, whose energy remains practically localized to a finite region.

The analytical solutions for $\xi_z(z)$ and $P(z)$ in the solar interior are (Evans & Roberts (1990)):

$$\xi_z(z) = A\frac{e^{-k(z+z_0)}}{\omega^4-g^2k^2}[(k\omega^2v_s^2(z)+gk^2v_s^2(z)-g\gamma\omega^2) \cdot U(-a,m+2,2k(z+z_0)) - 2ak\omega^2v_s^2(z)U(-a+1,m+3,2k(z+z_0))], \tag{10}$$

$$P(z) = A\frac{\rho_0(z)e^{-k(z+z_0)}}{\omega^4-g^2k^2}[(-v_s^2(z)\omega^4 - gkv_s^2(z)\omega^2 + g^2\gamma\omega^2)\cdot U(-a,m+2,2k(z+z_0)) + 2agkv_s^2(z)\omega^2U(-a+1,m+3,2k(z+z_0))]. \tag{11}$$

A is an arbitrary amplitude, U is a confluent hypergeometric function (Abramovitz & Stegun (1965)) and $a \equiv \frac{m\omega^2-gk(m+2)}{2gk}$.

The solutions in the corona are:

$$\xi_z(z) = \xi_{zc}\exp((-\frac{1}{2H}+\kappa)(z+L)),$$
$$P(z) = \rho_{0c}\xi_{zc}\left(\frac{C_1}{C_2} - \frac{D}{C_2}(-\frac{1}{2H}+\kappa)\right) \cdot \exp[(\frac{1}{2H}+\kappa)(z+L)], \tag{12}$$

with complex or positive real

$$\kappa \equiv \sqrt{\left(\frac{C_1}{D}+\frac{1}{2H}\right)^2-\frac{C_2C_3}{D^2}}. \quad (13)$$

ξ_{zc} is the displacement perturbation taken at z = -L, $H \equiv \frac{\mathcal{R}T_c}{g\mathcal{M}}\frac{1+\beta}{\beta}$ is the coronal pressure scale height.

The sound speed and the Alfvén speed are constant and the density falls off exponentially in the corona, hence κ is constant, and its value can be easily evaluated at z = -L.

From the definitions (5) and (13) it follows that the coefficient κ^2 can be written as a fraction, of which the nominator is a cubic function of ω^2:

$$\kappa^2 = -\frac{(\omega^2-\omega_I^2)(\omega^2-\omega_{II}^2)(\omega^2-\omega_{III}^2)}{(v_s^2+v_A^2)(\omega^2-\omega_A^2)(\omega^2-\omega_c^2)}. \quad (14)$$

Here ω_I^2, ω_{II}^2 and ω_{III}^2 denote the three yet unknown roots of the third order polynomial in ω^2.

For $k_y = 0$, one of these three roots, say ω_{III}, equals ω_A^2. Hence the expression for κ^2 can be simplified, and the denominator can be reduced to a quadratic function of ω^2:

$$\kappa^2 = -\frac{(\omega^2-\omega_I^2)(\omega^2-\omega_{II}^2)}{(v_s^2+v_A^2)(\omega^2-\omega_c^2)}. \quad (15)$$

Explicit expressions for ω_I^2 and ω_{II}^2 are:

$$\begin{aligned}\omega_I^2 &= \tfrac{1}{2}(k^2+\tfrac{1}{4H^2})(v_s^2(\text{-}L)+v_A^2(\text{-}L))\left(1-\sqrt{1-\lambda}\right),\\ \omega_{II}^2 &= \tfrac{1}{2}(k^2+\tfrac{1}{4H^2})(v_s^2(\text{-}L)+v_A^2(\text{-}L))\left(1+\sqrt{1-\lambda}\right),\end{aligned} \quad (16)$$

where

$$\lambda = \frac{4k^2[(k^2+\frac{1}{4H^2})v_s^2(\text{-}L)v_A^2(\text{-}L)+\frac{g}{H}v_s^2(\text{-}L)-g^2]}{(k^2+\frac{1}{4H^2})^2(v_A^2(\text{-}L)+v_s^2(\text{-}L))^2}. \quad (17)$$

To obtain the solution in the corona, we integrate Eq. (4) numerically from z = -L to z = 0. The solutions in the dissipative layer, around z_c and in two overlap regions above and below the dissipative layer can be derived following Tirry & Goossens (1996) and Tirry et al. (1998). Application of the continuity conditions for ξ_z and for $P + g\rho_0\xi_z$ yields the dispersion relation. For a given wave vector the dispersion relation has to be solved for the frequency ω.

3. Eigenmodes in absence of a magnetic field

The present and the following sections are devoted to the numerical solutions of the eigenvalue problem.

Observers prefer the cyclic frequency ν and the spherical degree l rather than the angular frequency $\omega(\equiv 2\pi\nu)$ and the horizontal wave number $k(\equiv\sqrt{l(l+1)}/R_\odot)$. This has led us to present the results in terms of ν and l.

As in Tirry et al. (1998), we take the following values for T_p = 4170 K, T_c/T_p = 80, L = 2 Mm, g=274 m s^{-2}, $R_\odot$ = 696 Mm, $\mathcal{M}$ = 1.3 g mol^{-1}, $\gamma = 5/3$, m=1.5.

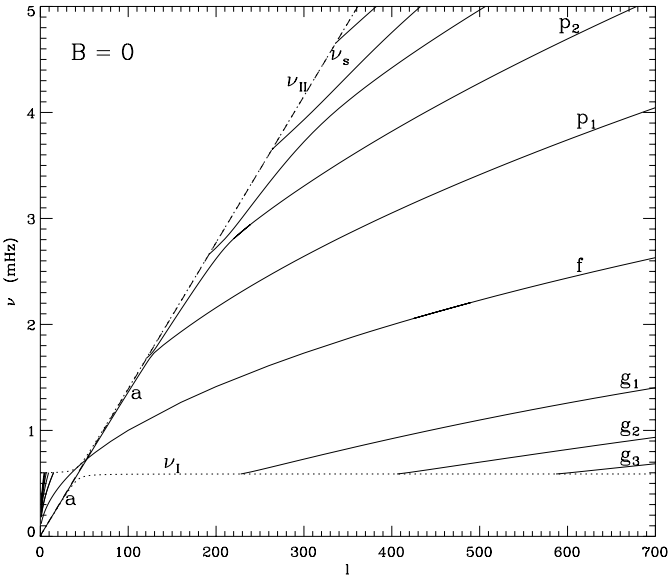

Fig. 2. The lower and upper cutoff frequencies (dotted lines), the sound frequency (dashed line), and the eigenfrequencies for the a- g- f- and p-modes (solid lines) as functions of the harmonic degree l in an absence of magnetic field

The aim of this paper is to understand how a simple chromospheric and coronal magnetic field affects the global solar oscillations. The oscillations of the non-magnetic model are the obvious starting point of our discussion.

3.1. Characteristic frequencies

Frequencies of eigenmodes of the non-magnetic solar model are plotted in Fig. 2. The oscillation modes which are evanescent in the corona exist between the lower and upper cutoff frequencies, ν_I and ν_{II}. The harmonic degree, l, ranges from 0 to 700. Modes below the lower cutoff frequency or above the upper cutoff frequency ($\nu < \nu_I$ or $\nu > \nu_{II}$) propagate in the corona. The energy of those waves is not confined to the sun, and we do not consider them as eigenmodes.

The asymptotic expressions for the cutoff frequencies for $l \ll \frac{R_\odot}{H_0}$ are:

$$\nu_I = \frac{\sqrt{\gamma-1}}{\pi\gamma}\frac{\sqrt{l(l+1)}}{R_\odot}v_s(\text{-}L),\ \ \nu_{II} = \frac{\gamma}{4\pi}\frac{g}{v_s(\text{-}L)}, \quad (18)$$

and for $l \gg \frac{R_\odot}{H_0}$:

$$\nu_I = \frac{\sqrt{\gamma-1}}{2\pi}\frac{g}{v_s(\text{-}L)},\ \ \nu_{II} = \frac{1}{2\pi}\frac{\sqrt{l(l+1)}}{R_\odot}v_s(\text{-}L). \quad (19)$$

Note that ν_I^2 for large l and ν_{II}^2 for small l are constant, however ν_I^2 for small l and ν_{II}^2 for large l vary as l(l+1). Hence ν_I for large l and ν_{II} for small l are basically linear functions of l. The actual variations of ν_I and ν_{II} follow closely their asymptotic approximations.

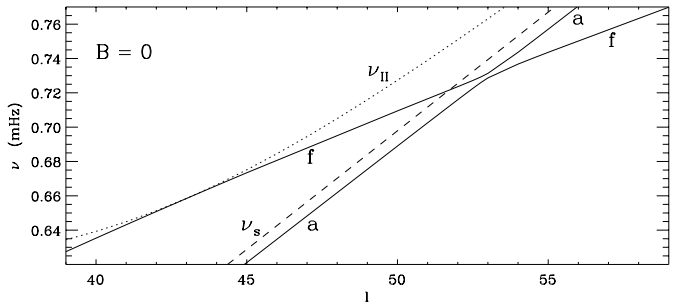

Fig. 3. Enlargement of a region in Fig. 2, showing the avoided crossing of the a-mode and the f-mode. The curve of the f-mode frequency turns up as an a-mode, while the curve of the a-mode turns down and becomes the f-mode.

The threshold value of the wave number where the difference between the cutoff frequencies attains its minimal value

$$l_{thr} = \frac{\sqrt{\gamma - 1}}{\gamma} \frac{R_\odot}{H}. \tag{20}$$

Here we have $l_{thr} \approx 45$. The relative difference of the cutoff frequencies for l_{thr} is

$$2\frac{\nu_{II} - \nu_I}{\nu_{II} + \nu_I}\bigg|_{l=l_{thr}} = \frac{2|2-\gamma|}{\sqrt{\gamma^2 + 12\gamma - 12}}. \tag{21}$$

For $\gamma = 5/3$ this difference is only 0.2, so the curves ν_I and ν_{II} in the (l, ν) plane follow closely their asymptotics.

The variation of ν_I and ν_{II} with l leads to a natural division of the (l, ν) plane into two parts. The first part corresponds to low degree modes ($l \leq 45$) and the second part to high degree modes ($l \geq 45$).

3.2. Global eigenmodes

Different types of modes can be distinguished in the frequency spectrum: p-modes (pressure-modes), the f-mode (fundamental mode) and g-modes (internal gravity modes).

In the low-l domain ($0 < l < 45$) we find a group of p-modes, the f-mode and the a-mode. The p-modes are terminated at the upper cutoff frequency, ν_{II}, while the f-mode frequency, ν_f, goes into the high-l domain ($l > 45$).

In addition, there is another mode in the low-l domain. The frequency of this mode is very close to the value of the sound frequency, ν_s. This eigenoscillation represents another type of acoustic mode, which is localized at the top of the solar interior. These properties suggest us to identify this mode as the Lamb mode, which is studied e.g. in Lamb (1932), Hasan& Christensen-Dalsgaard (1992) and Hindman & Zweibel (1994). We adopt the terminology introduced by Hindman & Zweibel (1994), who referred to this mode as the a-mode.

Since $\nu_{\rm a}$ increases steeply with l, the frequency of the a-mode would eventually cross the more gently increasing ν_f, ν_{p_1} and ν_{p_2}. However, there is not any actual crossing, although the separation between $\nu_{\rm a}$ and ν_f becomes very small at a particular point. As $\nu_{\rm a}$ moves further away from ν_s with increasing l, the avoided crossing of the modes becomes more and more apparent.

The complexity of the present model does not make it possible to give exact analytical expressions for the global mode frequencies. However, an estimate can be given for the critical harmonic degree for minimal separation between the ridges of the a- and the f-mode. The a-mode frequency can be approximated by the sound frequency and the f-mode frequency can be approximated by its theoretical value in a closed atmosphere (see e.g. Christensen-Dalsgaard (1994)):

$$\begin{aligned} \nu_a &= \frac{1}{2\pi}\frac{\sqrt{l(l+1)}}{R_\odot} v_s, \\ \nu_f &= \frac{1}{2\pi}\sqrt{\frac{\sqrt{l(l+1)}}{R_\odot}\, g}, \end{aligned} \tag{22}$$

with $v_s = \sqrt{\gamma \frac{\mathcal{R}}{\mathcal{M}} T_c}$. The threshold value for the harmonic degree where the difference between the frequencies of the a-mode and the f-mode is minimal can be obtained as

$$l = \frac{g\mathcal{M}R_\odot}{\gamma \mathcal{R} T_c}. \tag{23}$$

For the present model, this value is $l = 53.7$, in good agreement with the numerical result shown in Fig. 3. This figure shows the avoided crossing between the a-mode and the f-mode. The frequencies of the two modes come from the low-l domain, they nearly merge at about $l = 53$, where ν_f turns up and moves slightly below the sound frequency as the a-mode, while $\nu_{\rm a}$ turns down becoming the f-mode in the high-l domain.

Gravity modes can exist below the Brunt-Väisälä frequency, ν_g, which is defined by (Christensen-Dalsgaard (1994)):

$$\nu_g^2(z) = \frac{g}{4\pi^2}\left(\frac{d\ln\rho_0(z)}{dz} - \frac{g}{v_s^2(z)}\right) \tag{24}$$

The g-modes that are studied in helioseismology (e.g. Christensen-Dalsgaard (1994), Hindman & Zweibel (1994)) are mainly confined in the solar interior. The solar interior in the present model is in convective equilibrium. The Brunt-Väisälä frequency equals zero due to the choice of an adiabatic temperature profile. Therefore, there are not any g-modes associated with the solar interior. However, ν_g^2 is positive in the transition layer, hence gravity modes can exist in the present atmospheric model as well.

The maximal value of ν_g is about 17.4 mHz, thus it is not plotted in Fig. 2. The solar interior is considered neutrally stable to convection, thus $\nu_g(z > 0) \equiv 0$. The Brunt-Väisälä frequency does not depend on the harmonic degree, and it takes its maximal value in the transition layer, forming a cavity for the internal gravity modes.

3.3. Spatial solutions

Typical spatial solutions are plotted in Fig. 4 for the f-mode and for the first two p-modes and in Fig. 5 for the first three g-modes for $l = 600$. The p-modes show an oscillatory behaviour in the vicinity of the top of the solar interior ($z \approx 0$).

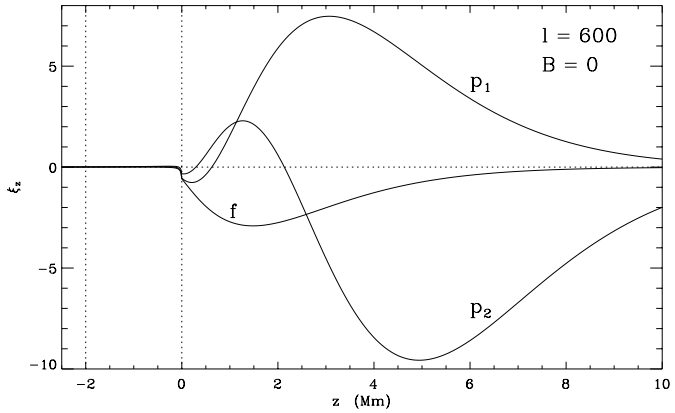

Fig. 4. Typical spatial vertical solutions for the Lagrangian displacement for the f-mode and for the two first p-modes

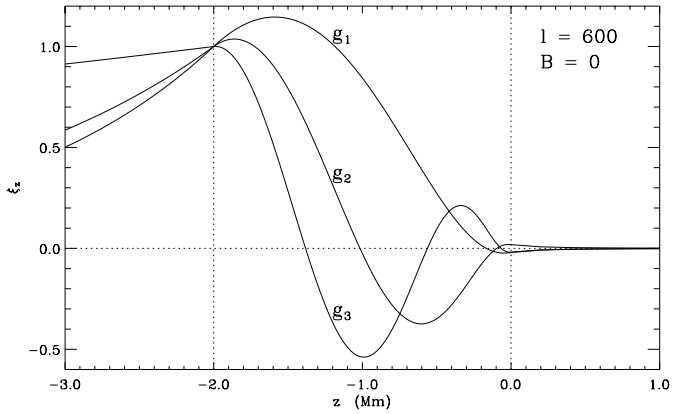

Fig. 5. Typical spatial eigenvalue solutions for the first three g-modes, normalized by their amplitudes at $z = -L$.

The nodes of the g-modes are located in the transition layer, in other words, the oscillations are trapped in the transition layer, as $\nu_g^2(z)$ is positive only there.

In the solar interior (z>0) and in the corona (z<-L) the g-modes are evanescent. There are no g-modes in models without the transition layer.

The g-modes are anti-Sturmian: the number of nodes decreases with increasing frequency. For p-modes, Fig. 4 displays a Sturmian behaviour: the number of nodes increases with increasing frequency.

4. Effect of the magnetic field parallel to the horizontal propagation, $\theta = 0$

Let us now see what happens to the eigenoscillations when we add a magnetic field to the solar atmosphere. The analysis in the present paper is restricted to oscillation modes that propagate parallel to the magnetic field ($k_y = 0$).

In an investigation of the influence of a horizontal stratified magnetic field on waves, it is instructive to know how the characteristic frequencies depend on the strength of the magnetic field. The magnetic field strength can be measured by its value at the base of the transition layer: $B_p \equiv B_0(z = 0)$.

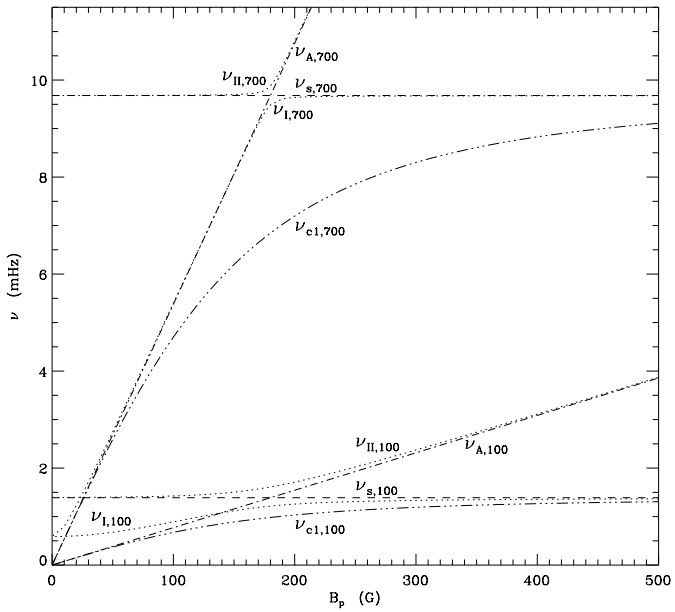

Fig. 6. The lower and upper cutoff frequencies (dotted lines), the sound frequency (dashed line), the Alfvén and cusp frequencies (dash-dot lines) taken at the base of the corona, z = -L, as functions of the magnetic field for $l = 100$ and $l = 700$.

4.1. Characteristic frequencies

For eigenoscillations with a horizontal wave vector parallel to the magnetic field, Eq. (15) implies that the spectrum has three cutoff frequencies, ν_I, ν_{II} and ν_{c1}, as $\kappa^2(\nu)$ changes its sign at these values of ν. The minimal and maximal values of the cusp frequency are denoted as ν_{c0} and ν_{c1} respectively.

Eigenmodes, with real frequencies, lie between ν_{II} and the maximum of ν_I and ν_{c1}, whereas quasimodes, with complex frequencies, can be found below the minimum of ν_I and ν_{c1}.

Fig. 6 shows the characteristic frequencies for two different degrees, $l = 100$ and $l = 700$.

For weak magnetic field strengths, the upper cutoff frequency, ν_{II}, is almost equal to the constant sound frequency, ν_s. With increasing magnetic field strength, the lower cutoff frequency, ν_I, approaches the upper cutoff frequency, ν_{II}.

Their closest encounter occurs at around $\beta = 1$, where the gas pressure is equal to the magnetic pressure. The value $\beta = 1$ corresponds to $B_p \approx$197 G. For a stronger magnetic field, the two cutoff frequencies move away from each other, and approach their asymptotic variations, which are the constant sound frequency, ν_s, for ν_I and the linearly increasing Alfvén frequency, ν_A, for ν_{II}:

$$\begin{aligned} \lim_{B_p\to\infty} \nu_I &= \frac{\sqrt{l(l+1)}}{R_\odot} v_s(\text{-}L), \\ \lim_{B_p\to\infty} \nu_{II} &= \frac{\sqrt{l(l+1)}}{R_\odot} v_A(\text{-}L). \end{aligned} \tag{25}$$

The Brunt-Väisälä frequency in a magnetic field is (Chen and Lykoudis (1972)):

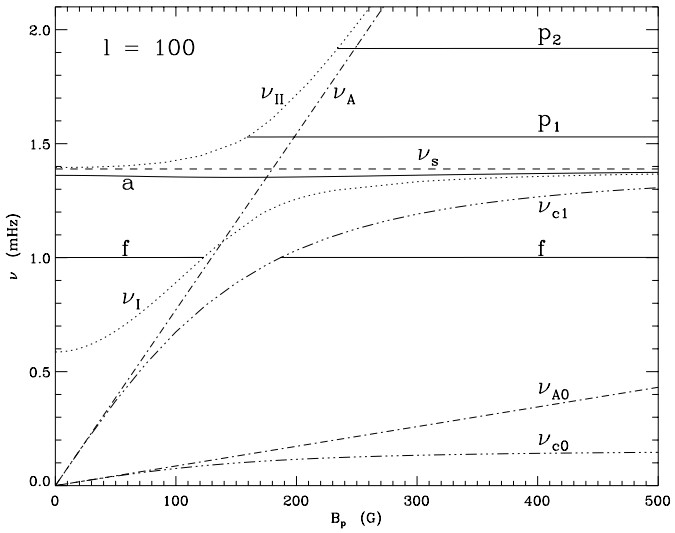

Fig. 7. Variation of eigenfrequencies as a function of the base magnetic field for spherical degree of $l = 100$. Between the cutoff frequencies ν_{II} and ν_I (dotted lines) the eigenmodes (straight lines) are real, while the frequency of the f-mode is complex in the slow continuum, i.e. between ν_{c1} and ν_{c0} (dash-dot lines).

$$\nu_g^2(z) = \frac{g}{4\pi^2}\left(\frac{d\ln\rho_0(z)}{dz} - \frac{g}{v_s^2(z)+v_A^2(z)}\right). \qquad (26)$$

It is zero in the convection zone, and only decreases slightly with the magnetic field in the transition layer.

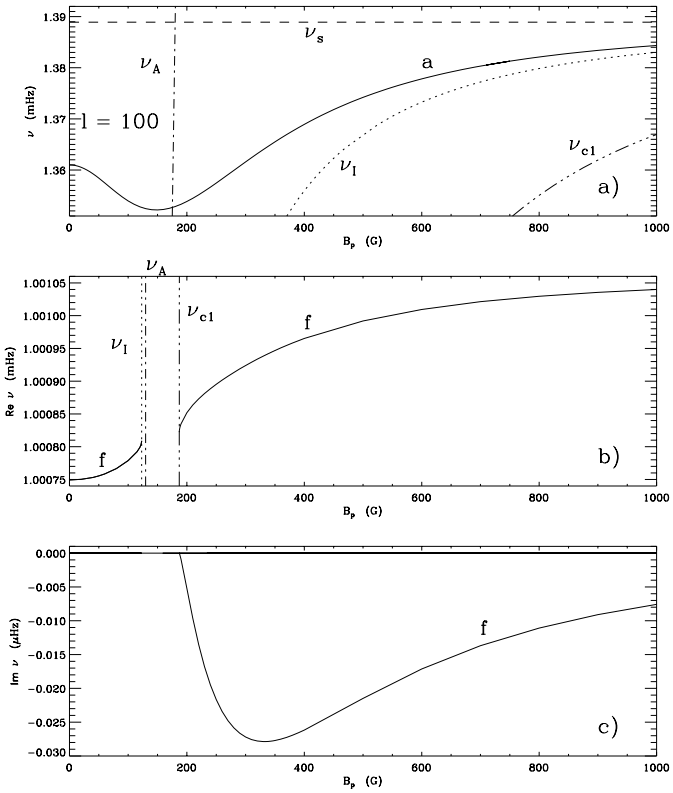

Fig. 8. a, **b** Detailed view of the a-mode and the f-mode as a function of the magnetic field. **c** The damping rate of the f-mode due to the coupling to the local slow oscillations.

4.2. Variation as a function of the magnetic field strength, for $l = 100$

Let us study how the frequencies of the eigenmodes change with the magnetic field strength for a given spherical degree. Fig. 7 shows eigenmodes for $l = 100$, which corresponds to $k \approx 0.14$ Mm^{-1}. The magnetic field at the base of the transition layer changes from 0 to 500 G.

For $B = 0$, only two modes exist for $l = 100$: the f-mode and the a-mode. The p-modes of low order come into existence when the magnetic field strength is increased. The frequencies of these p-modes increase with the magnetic field.

The frequency of the a-mode lies between the constant sound frequency, ν_s, and the lower cutoff, ν_I. Fig. 7 shows that the frequency of the a-mode is rather insensitive to the strength of the magnetic field. That there is indeed a week dependence of the frequency of the a-mode on the strength of the magnetic field is shown in Fig. 8a, where the scale on the frequency axis is expanded compared to that of Fig. 7. For a weak magnetic field, the shift of the a-mode frequency is negative, however, for a strong field (B_p>293 G), the shift is slightly positive. All in all, the variation in the frequency of the a-mode is less than four percent over a range of 1,000 G. Fig. 8b gives an enlarged view of the dependence of the f-mode frequency on the strength of the magnetic field. The frequency of the f-mode increases with increasing magnetic field strength, reaches the cutoff line, ν_I, and disappears at a field strength of approximately 123 G. It subsequently reappears in the slow continuum at 187 G as a quasimode. There is an interval of the magnetic field strength in which the f-mode does not exist. In the slow continuum, i.e. in the frequency region between ν_{c0} and ν_{c1}, the f-mode couples to the local slow continuum modes at height $z = z_c$, and its frequency becomes complex. (Note that $\nu_{c0} \equiv \nu_c(z$=0) and $\nu_{c1} \equiv \nu_c(z$=-$L)$ for $B_0(z$=0$) = B_p$.) The real part of the f-mode increases in the slow continuum less and less steeply. The imaginary part of the f-mode (see Fig. 8c) is negative and its absolute value is much smaller (10^5 times less) than its real part, so that the f-mode is actually very weakly damped (compare Fig. 8b and Fig. 8c). The damping of the f-mode is maximal at $B_p \approx 332$ G.

4.3. Variation as a function of the magnetic field strength, for $l = 700$

For eigenoscillations with smaller wave lengths the picture is even more complicated. Fig. 9 is for $l = 700$, which corresponds to $k \approx 1$ Mm^{-1}. In addition to the f-mode the first g-mode and several p-modes couple to local modes in the slow continuum for a rather weak magnetic field. The modes in the slow continuum are quasimodes with small damping rate.

They can split into several discrete modes, and they can disappear at given B_p. Fig. 9 shows how the g-modes, the f-

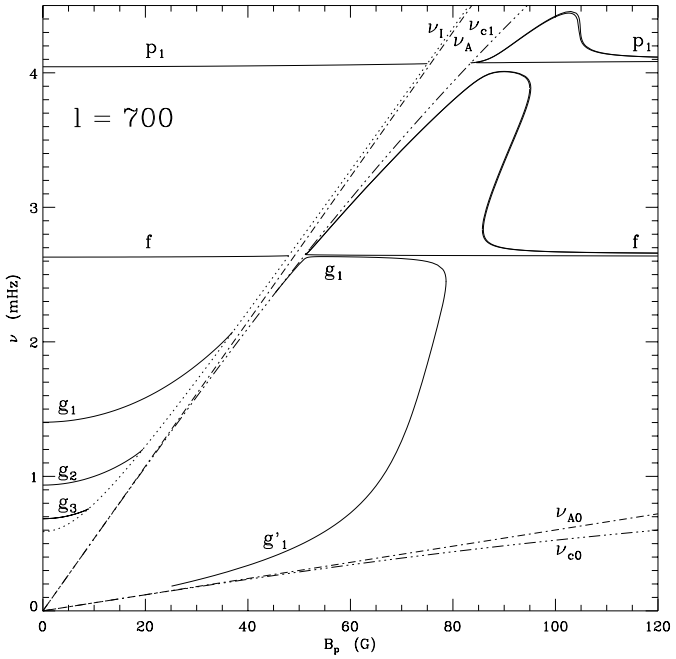

Fig. 9. Same as Fig. 7 but for $l = 700$

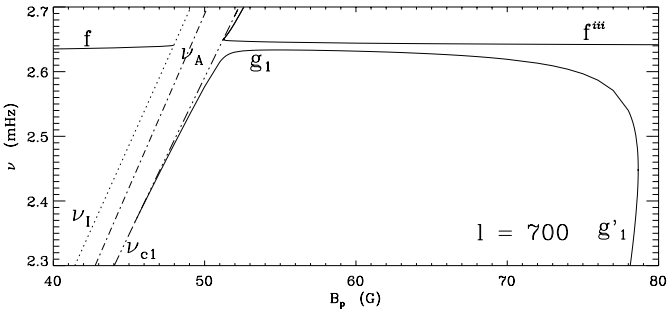

Fig. 10. An enlargement of Fig. 9 concentrating on the g_1-mode in the slow continuum.

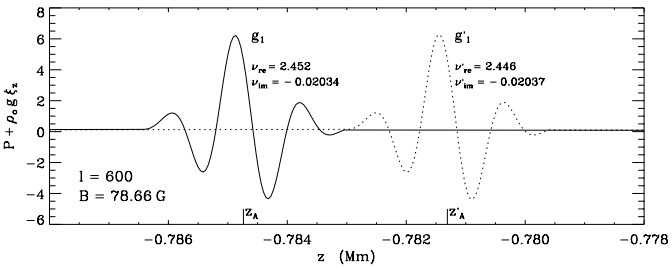

Fig. 11. Spatial solutions of the total pressure perturbation for the g_1- and g_1'-mode around the slow resonant points, z_A and z_A'

mode and the p_1-mode are terminated at the lower cutoff, ν_I for increasing B_p.

g-modes. The g_1-mode exists also in the slow continuum. The variation of the real part of the frequency of the g_1-mode frequency is enlarged in Fig. 10. The mode enters the slow continuum at about $B_p = 46$ G, and the real part of ν_{g_1} increases up to near the f-mode frequency, and then decreases when B_p is further increased. In Fig. 10 there is another mode in the gravity part of the spectrum, which we call the g'$_1$-mode for reasons obvious in a moment. Initially, its frequency is close to the lower boundary of the slow continuum, ν_{c0}, and increases with the magnetic strength (see Fig. 9). For higher field strengths, $\nu_{g_1'}$ approaches the g_1-mode, and both the g'$_1$-mode and the g_1-mode disappear before reaching $B_p = 79$ G.

The damping rate of the g_1- and g'$_1$-mode due to the interaction with the local slow oscillation can be seen in Fig. 14. The imaginary part of the eigenfrequency is plotted as a function of the real part. The real part of the g'$_1$-mode frequency goes to zero with decreasing l (see also Fig. 9). Fig. 14 shows that the ratio between the real and imaginary part of the mode frequency becomes smaller and smaller as l decreases. The assumption that $\omega_r \gg |\omega_i|$ is not satisfied for the g'$_1$-mode for small values of l. Physically, it results in very weakly evanescent amplitude of the mode in the corona, because $\kappa_r \gg |\kappa_i|$ is neither satisfied. Mathematically, it causes numerical difficulties. That is the reason why the ridge of the g'$_1$-mode ends at $\nu = 0.2$ mHz and for $l = 25$.

Spatial solutions for the g_1-mode and the g'$_1$-mode are plotted in Fig. 11. They are very similar. The only visible difference is the position of the slow resonant layers.

The spatial solutions for the g'$_1$-mode and for the g_1-modes with frequencies in the slow continuum have six nodes. One of the six nodes occurs in the ideal region. The other five nodes are located in the dissipative layer, around the resonant position, z_c. This strongly oscillatory behaviour with small wavelength in the dissipative layer is due to the interaction with the slow continuum modes.

Continuation of the lower g-modes, g_2 and g_3, was not found in the slow continuum.

f-modes. The behaviour of the f-mode in the slow continuum is even more complicated than that of the g_1-mode. All in all we found eight f-type modes in the slow continuum with a minimal number of one and a maximal number of seven being present for a given magnetic field strength.

Our original notation of these f-type modes is f and f^i to f^{vii}. The f-, f^{ii}- and f^{iii}-modes follow the initial appearance of the f-mode in the slow continuum. It turns out that the f-mode is the first part of an inverted S-shaped curve in the (B_p, ν) plane defined by three f-modes: f, f^v and f^{vi}.

The same phenomenon is found for the f^{ii}-mode. Here the inverted S-shaped curve is defined by the modes f^{ii}, f^{iv} and f^{vii}. At a very large magnetic field, $B_p \approx 11,700$ G – which is not shown in Fig. 9 – the frequencies of the two modes, f^{iii} and f^{vii}, match and the modes are terminated for stronger magnetic field. Hence, the curve consisting of the modes f^{ii}, f^{iii}, f^{iv} and f^{vii} forms a loop. Hereafter, we refer to this frequency ridge as the f-loop.

Let us now have a more detailed look at the f-type modes.

In the interval 86 G $\leq B_p \leq$ 95 G there are seven f-modes at the same strength of the magnetic field. The distances between the different f-mode frequencies are very small in some cases, thus two regions of the slow continuum are enlarged in Fig. 12a and 12b.

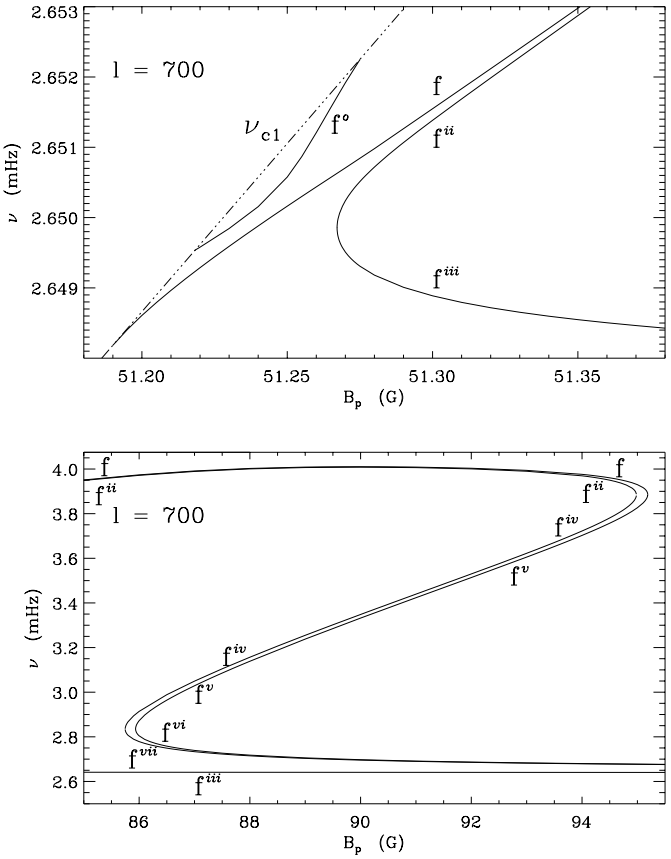

Fig. 12a and b. Two enlargements of Fig. 9. **a** This figure shows how the f-mode enters the slow continuum. Two new modes, f^{ii} and f^{iii}, emerge for $B_p = 51.27$ G. The mode labeled as f^o exist for only a short interval of B_p. **b** The region where seven f-type modes exist for the same magnetic field strength.

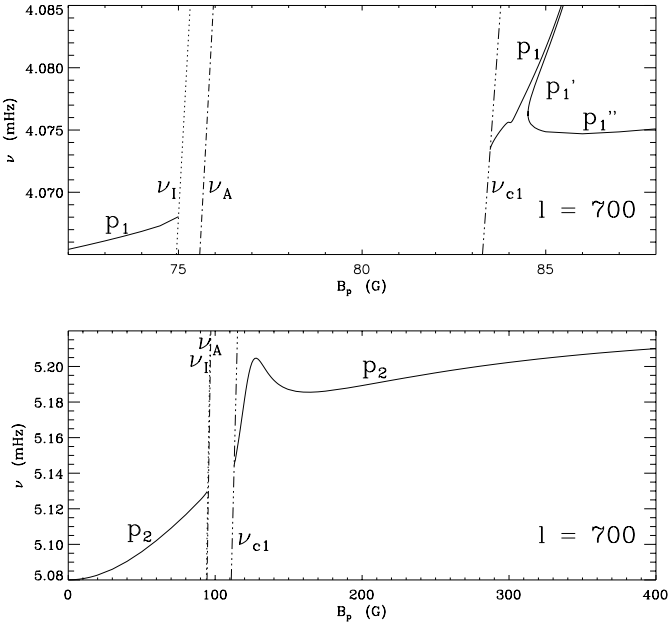

Fig. 13a and b. Two enlarged parts of Fig. 9. No eigenfrequency exists between the lower cutoff frequency, ν_I, and the upper boundary of the slow continuum, ν_{c1}. **a** The variation of the p_1-mode frequency and emergence of two other p_1-type modes, p_1' and p_1''. **b** The frequency of the p_2-mode.

First, we follow the f-mode. This mode enters the slow continuum at $B_p \approx 51.2G$. Near the top of the slow continuum, ν_{c1}, the real part of the f-mode frequency, ν_f, increases (Fig. 12a), reaching its maximum at $B_p \approx 90$ G (Fig. 9 and Fig. 12b). This curve is terminated at $B_p \approx 95$ G, together with the f^v-mode, that exists only for $B_p \geq 86$ G. The lower continuation of the f^v-mode is the f^{vi}-mode. This mode starts around $B_p = 86$ G and extends in the domain of strong magnetic field. (After its minimum at $B_p \approx 156$ G, its frequency keeps on increasing slightly.)

Above f we find f^o, originating at the upper boundary of the slow continuum. It is displayed in Fig. 12a. This member of the f-type modes exists only in a very small interval, between $B_p \approx 51.22$ G and $B_p \approx 51.28$ G. After a short increase it turns back to ν_{c1} and disappears there. The spatial solution of this mode has six nodes in the dissipative layer (around z_c), and it has no node in the ideal region, as for the f-mode above the slow continuum (Fig. 4).

Fig. 12a also shows that below ν_f, at around $B_p = 51.27$ G, two additional modes, f^{ii} and f^{iii}, appear, which do not exist for a weaker magnetic field.

The f^{ii} mode disappears together with the f^{iv} mode, which exists between $B_p = 85.7$ G and $B_p = 95.2$ G. The f^{iv} mode appears together with the f^{vii} mode.

The spatial solutions of the f^{ii}-, f^{iii}-, f^{iv}- and f^{vii}-modes, also show the properties of the f-mode: they have no node in the ideal region. In the dissipative layer, the spatial eigenfunctions for the vertical component of the Lagrengian displacement have eight nodes contrary to the f^i, f^v and f^{vi} modes, which have only six nodes in the dissipative layer. The fact that the relevant difference between the two types of f-mode is the number of nodes in the dissipative layer suggests that the existence of several f-modes is basically caused by the resonant coupling to the local slow mode.

Summing up, instead of a smooth variation of the frequency of the f-mode with B_p in the slow continuum we have found a) a short curve f^o, originating and ending at the upper boundary of the slow continuum. b) An s-shaped curve which begins at ν_{c1} and extends unboundedly in the domain of strong magnetic field. The modes belonging to this s-curve (f, f^v and f^{vi}), have the common feature that their solutions have six nodes in the dissipative region. c) An s-shaped curve or better a loop if we go to very strong magnetic fields consisting of the f^{ii}-, f^{iii}-, f^{iv}- and f^{vii}-modes. In the dissipative region, the modes corresponding to this f-loop oscillate with eight nodes.

The imaginary parts of the f-modes are shown in Fig. 14. The f^o-mode has a very small damping rate (order of nHz), which is not visible in Fig. 14. The damping rate of the modes which belong to the s-curve extends to 7μHz. This strong damping rate of the f-mode is reached for a magnetic field strength of $B_p \approx 433$ G. The imaginary part of the quasimode frequencies

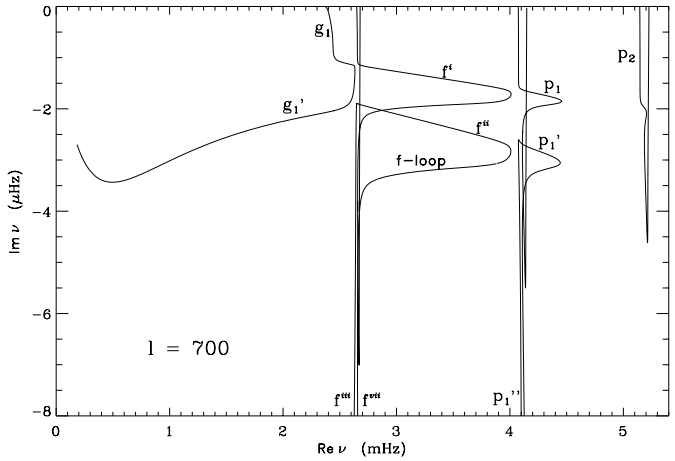

Fig. 14. Damping rate of some modes in the slow continuum as function of the real part of the mode frequencies for a large interval of the magnetic field.

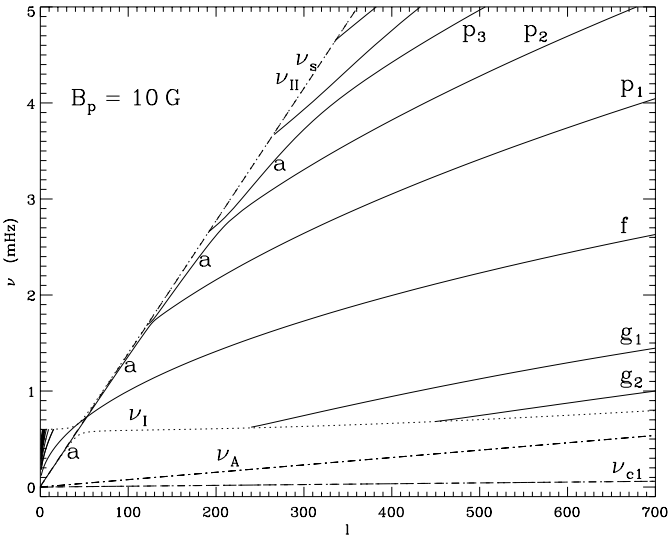

Fig. 15. Mode frequencies for a weak magnetic field as a function of l. The modes are located between the lower and the upper cutoff frequencies.

in Fig. 14 are plotted only from -8 μHz, however, the damping rate of the modes which belong to the f-loop takes values up to even 47 μHz. This maximal value is related to an unrealistically strong magnetic field of $B_p \approx 11,700$ G. Generally, the damping for the modes which belong to the f-loop is stronger than that for the modes which belong to the S-curve.

p-modes. As a result of the resonant coupling between the global first p-mode and the local slow oscillations, there are three p_1-type modes, p_1, p'_1 and p''_1, in the slow continuum. Fig. 13a enlarges a part of Fig. 9 to show how the p_1-mode is terminated when it reaches the lower cutoff frequency, ν_I, and how it enters the slow continuum at ν_{c1}. It can be seen in Fig. 9 that the frequency, ν_{p_1} is a function of B_p with one local maximum at $B_p \approx 103$ G. It has also one local minimum, at about $B_p = 143$ G.

The curve that contains p'_1 and p''_1 exists in the interval for B_p from 84.5 G to 4,473 G (however, the upper limit is beyond the relevant range for the sun, and it is not plotted in Fig. 9).

As to the damping rate shown in Fig. 14, the curves belonging to the p_1-mode have similar shapes as those of the f-mode, but generally, the damping of the first p-mode is smaller than that of the f-mode.

For the p_2-mode in the slow continuum only one eigenfrequency was found for each value of the magnetic field. The real part of ν_{p_2} is plotted in Fig. 13b. After a local maximum for $B_p = 128$ G and a local minimum for $B_p = 165$ G, it increases slowly getting closer to its asymptotic value in the limit of $B \to \infty$. The imaginary part of the p_2-mode can be seen in Fig. 14.

4.4. Variation as a function of the spherical harmonic degree, for $B_p = 10$ G

How do the eigenfrequencies vary as a function of l for a given value of the magnetic field? Fig. 15 describes the case of $B_p = 10$ G. An apparent change in comparison with the field free case (Fig. 2) is that the g_3-mode does not exist for $l \leq 700$.

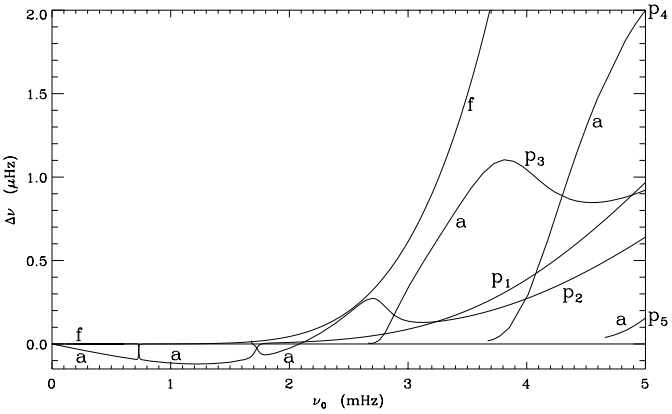

Fig. 16. Frequency shifts for $B_p = 10$ G. The frequency on the horizontal axis is that of a non-magnetic sun. The shifts of the p_2- and the p_3-modes have notable maxima at 2.7 mHz and at 3.9 mHz, respectively.

The modes are located between the lower and the upper cutoff frequencies. The eigenmodes propagating parallel to the magnetic field lines do not couple to the Alfvén continuum modes. They could couple to the local slow oscillations, however, we did not find eigenfrequencies in the slow continuum for $l \leq 700$.

As in the non-magnetic case, the frequency of the a-mode increases from $l = 0$, where it is between the sound frequency and the lower cutoff frequency, and approaches the frequency of the f-mode and the p_1-modes but avoids crossing them.

As the frequency increases, the a-mode moves away from the sound frequency.

From an observational point of view it is interesting to see how the frequencies of the eigenmodes are shifted due to the magnetic field.

In Fig. 16, the frequency shift, $\nu(B_p$=10G$) - \nu(B$=0), is plotted, related to the eigenfrequencies in the field free medium,

$\nu_0 \equiv \nu(B{=}0)$. The frequency shift is positive for all modes except for the a-mode with frequency less than 2 mHz. The avoided crossings of the a-mode with the p_2- and the p_3-modes occur at $\nu \approx 2.8$ mHz and $\nu \approx 3.9$ mHz. At these values the shifts $\Delta\nu_{p_2}(\nu)$ and $\Delta\nu_{p_3}(\nu)$ have local maxima. The labels p_4 and p_5 to the right of the panel indicate that the two a-modes become respectively the p_4-mode and the p_5-mode on larger frequencies. The frequency shifts for g-modes cannot be seen in the plot, because they are more than one order larger.

4.5. *Variation as a function of the spherical harmonic degree, for $B_p = 100$ G*

The characteristic frequencies ν_I and ν_{c1} increase with increasing magnetic field strength for given l (see Fig. 6). Therefore more modes enter the slow continuum, where the eigenfrequencies become complex. The real part of the eigenfrequencies for $l \leq 700$ and $B_p = 100$ G is plotted in Fig. 17. For this strong magnetic field no g-modes are found (compare with Fig. 9).

f-modes. The f-mode and the p_1-mode enter the slow continuum. We found five f-type modes in the slow continuum with a minimal number of one and a maximal number of three being present for a given value of the spherical harmonic. Three sections of the f-mode are enlarged in Fig. 18 in order to figure out the double 180°-bend of the curve related to the f-mode frequency, that is another example of the mode appearance and disappearance by the interaction with the local slow mode. The f-, f'- and f"-modes define an S-shaped curve in the (l, ν) plane. The S-shaped curve cannot be recognized in one panel because the frequencies of the f-, f'- and f"-modes are very close together. Combination of Fig. 18a and Fig. 18b reveals the S-form of the frequency ridge. Due to the appearance of two f-type mode, f^i and f^{ii} (Fig. 18a), and the disappearance of f and f^i (Fig. 18b), the spectrum has three f-type modes in the interval of $306.5 < l < 346.5$. For $l > 363.5$, two additional modes, f^{iii} and f^{iv}, appear, resulting in another triplet of the f-mode (Fig. 18c). The real parts of the frequency of the modes f^{ii}, f^{iii} and f^{iv} are very close to each other, hence they can be seen separately only in a huge enlargement. The triplet, f^{ii}, f^{iii} and f^{iv}, with $l = 700$ can be also found in Fig. 9 and in its enlarged region Fig. 12b, as the three modes labeled as f^{iii}, f^{vi} and f^{vii}, respectively.

p-modes. The p_1-mode enters the slow continuum at about $l = 521.5$, as it is enlarged in Fig. 19a. In addition to the original p_1-mode, two modes, p_1' and p_1'', appear at about $l = 545$. The difference between the frequencies of p_1 and p_1', are very small. With increasing l, p_1 and p_1' approach ν_{c1} (see Fig. 19b), in much the same way as the a-mode increases along ν_s. For the p_2-mode, we find a similar phenomenon. In addition to the original p_2-mode, two modes, p_2' and p_2'', appear. The separation between the frequencies of p_2 and p_2', are very small, and with increasing l, p_2 and p_2' approach ν_{c1}, while p_2'' together with p_1 and p_1' turn away from the upper boundary of the slow continuum.

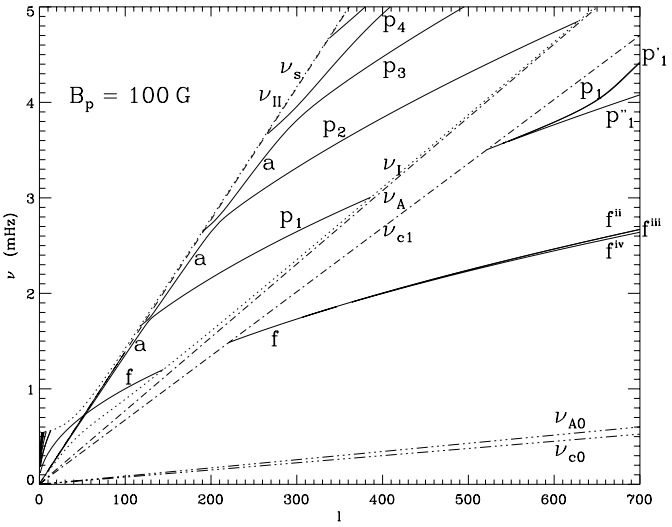

Fig. 17. Frequency spectrum as a function of the harmonic degree for $B_p = 100$ G. The eigenmodes, with real frequencies, are between the cutoff frequencies, ν_I and ν_{II}, while the quasimodes, with complex frequencies, exist in the slow continuum, between ν_{c1} and ν_{c0}.

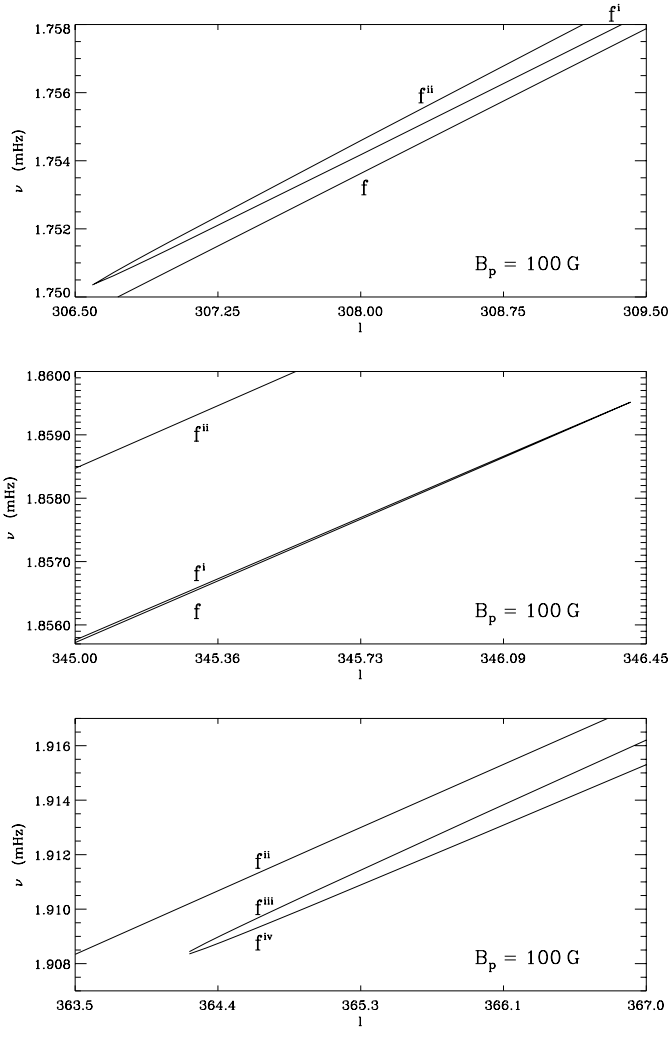

Fig. 18. The f-mode in the slow continuum with increasing l.

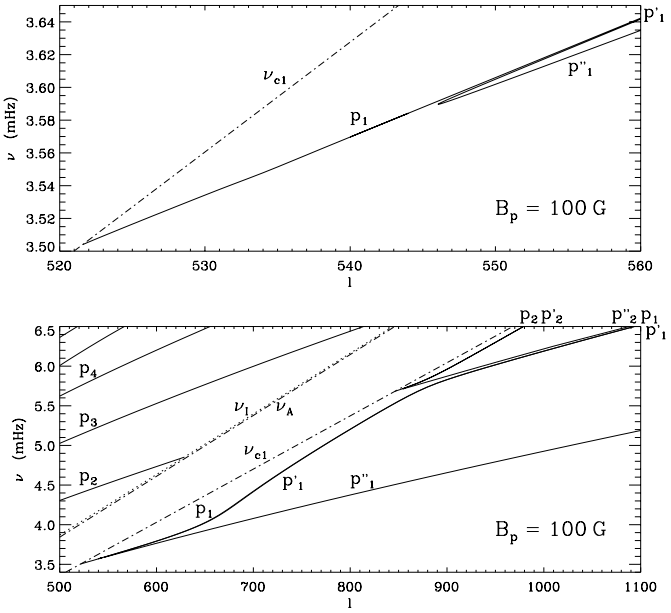

Fig. 19. The first and second p-modes in the slow continuum.

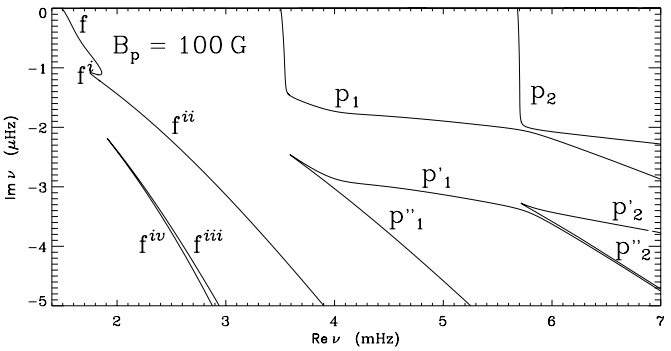

Fig. 20. The damping rate of f- and p-modes, caused by the coupling to the local slow modes.

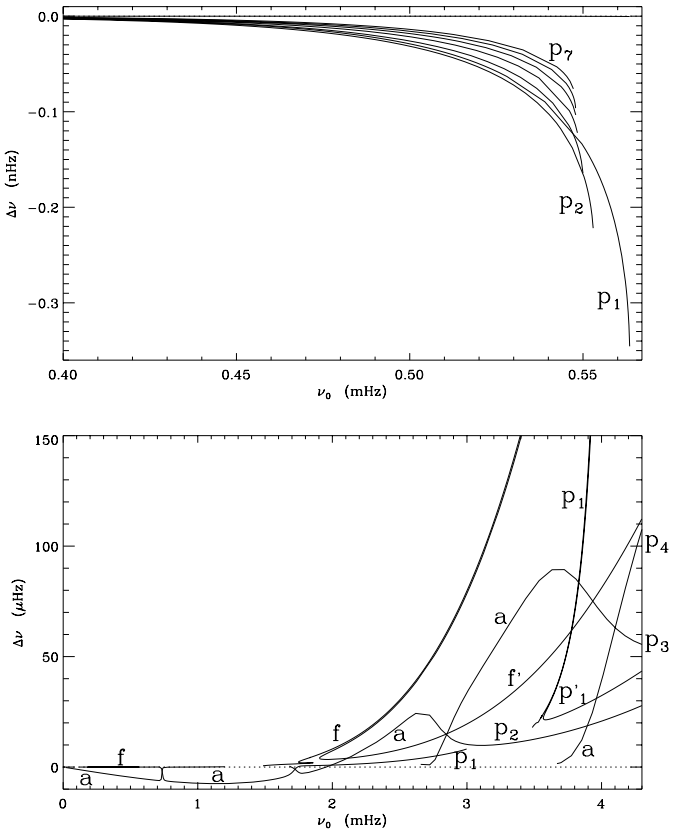

Fig. 21a and b. Frequency shifts of the oscillation modes: $\Delta\nu \equiv \nu(B_p$=100G)-$\nu(B$=0) as a function of $\nu(B$=0) **a** The shift in the low-l domain **b** The shift in the higher-l domain. The shift of p_2 and p_3 have maxima at 2.7 mHz and at 3.9 mHz.

The imaginary parts of the f-modes and of the first and second p-modes are plotted for a large interval of l in Fig. 20, as functions of Re ν.

The frequency shifts due to the chromospheric and coronal magnetic field are shown in Fig. 21. Shifts for modes with small wave numbers (l<20) are less than 1 nHz (Fig. 20a). In Fig. 20b, as for $B_p = 10$ G (Fig. 16), there are two local maxima in the frequency shifts for the second and third p-modes. The frequency shift has a maximum at $\nu = 2.7$ mHz for p_2, and at $\nu = 3.7$ mHz for p_3. In this case the shifts are two order larger than for $B_p = 10$ G.

5. Discussion and conclusion

In the present paper we have analysed how a chromospheric and coronal magnetic field influences the frequencies of global solar oscillations. The present paper uses the same three layer model as in Tirry et al. (1998). The solar interior for the p-mode cavity is represented by a polytrope. The magnetic field is ignored there as the gas pressure dominates there. The decreasing temperature is approximated by a linear function. The solar corona is modeled as a semi-infinite isothermal layer embedded in a uniform horizontal magnetic field. The model applied in Campbell & Roberts (1989) consists of these two layers. Tirry et al. (1998) have extended that model by adding a third layer between the two ones in which the Alfvén speed and the speed of sound increase linearly to their maximal values keeping the plasma-β constant. The reason for this choice is its mathematical simplicity and the absence of observed profiles of the Alfvén speed in that region. The thickness of the transition layer was fixed at $L = 2$ Mm, because this is the approximate distance on which the temperature in the solar atmosphere increases from its minimum to its coronal value. The magnetic field is taken horizontal to model the fanning out of the field lines changing from separated flux tubes to a magnetic canopy that fills the top of the photosphere. The model is a strong idealization in the sense that the temperature minimum coincides with the base of the magnetic layer. The constant Alfvén speed and the exponentially decaying density profile result in a very rapidly decreasing magnetic field in the corona. That is also far from the observations. However, the model provides us with a ba-

sis for understanding the magnetic effects on the solar global oscillations.

The thickness of the transition layer and the temperature ratio are fixed at $L = 2$ Mm and $T_c/T_p = 80$, respectively, throughout the paper.

Two cross sections of our numerical results are presented. First, the mode frequencies were given as functions of the magnetic field strength taken at $z =$ -L, B_p, for fixed values of the spherical degree ($l = 100$ and 700). This view can be related to the time evolution of the observed mode frequencies if the time dependence of the magnetic field is a simple function. Second, the value of the magnetic field was fixed at 10 G and 100 G, and the mode frequencies were plotted for an interval of l.

For given l and B_p, discrete eigenfrequencies can be distinguished far from the cutoff frequencies, and they can unambiguously be classified as the f-mode, a g-mode or a p-mode of given radial order. On the other hand, near the cutoff frequency lines, there is no strict separation between the different types of modes. Eigenmodes – instead of crossing each other – change character.

The eigenfunctions of the f- and p-modes oscillate below the photosphere. The p-modes show Sturmian behaviour. A p-mode of higher frequency has more nodes than another p-mode of lower frequency.

Gravity modes studied in helioseismology are trapped in a cavity with the turning point positions determined by the condition $\omega_g = \omega$ where ω_g is the well known Brunt-Väisälä frequency. At low frequencies this gives rise to one turning point very close to the centre of the sun, and a second one just below the base of the convection zone. At higher frequencies the upper turning point is shifted deeper in the sun and the gravity modes are trapped in the deep interior of the sun.

In the present model the Brunt-Väisälä frequency has been put equal to zero ($\omega_g = 0$) below the photosphere so that the classic gravity modes are absent. The density and pressure variations in the equilibrium model of the chromosphere lead to a positive Brunt-Väisälä frequency ($\omega_g > 0$) there, so that there is a cavity for gravity modes in the chromosphere. Hence the gravity modes in the present paper are chromospheric gravity modes. Their spectrum is anti-Sturmian just as that of the classic internal gravity modes and they are trapped in a cavity with the two turning point positions determined by the condition $\omega_g = \omega$.

This set of modes is definitely interesting and it is worth extending their analysis. Classifying these modes by their absorption coefficients, possible amplitudes, polarization of frequency bands is a task for another work.

The low-frequency oscillations have still not definitely observed, hence there is no observational evidence of the g-modes. Contrary to the f- and p-modes, the chromospheric gravity modes do not exist in strong magnetic fields. This can be a possible reason why g-modes have not yet been observed among the solar oscillations. Another possibility is that g-modes are easily transformed into other modes making it hard to observe them.

In the present paper the wave propagation was chosen parallel to the magnetic field lines, and the global modes do not interact with the local Alfvén oscillation mode. However, the global modes couple to the local slow modes. In the slow continuum the coupling of global eigenmodes to local slow modes changes the eigenmodes to quasimodes with complex frequency.

For given values of the magnetic field, we have plotted the frequency shifts of the modes as a function of the eigenfrequencies in field free case for a wide interval of the spherical degree. The frequency shifts are presented for the individual modes instead of averaging over the modes, although observational articles give only averaged curves. We did not do any averaging, because the lines obtained by averaging over the mode frequencies depend strongly on which mode or frequency domain is taken into account and on the strength of the magnetic field. A lot of information would be lost by averaging. Additionally, we cannot estimate how strong the averaged magnetic field was in the corona in 1988. Moreover, the solar corona was magnetically dominated not only in 1988 but in 1986. This means that that case cannot be treated as field free. The point of the comparison is only that the mentiond plots in both papers illustrate frequency shifts due to an increase in the strength of the magnetic field.

For $B_p = 10$ G and 100 G, the frequency shifts of the p-modes of radial order two and three have a local maximum at around 2.8 mHz and 3.9 mHz, respectively. The turnover around 3.9 mHz can also be seen in Fig. 2.a in paper by Libbrecht & Woodard (1990). They measured frequency shifts between 1986 and 1988. The magnetic cycle had reached a considerable amplitude by 1988, while 1986 was near solar minimum. Libbrecht and Woodard have plotted the shift $\nu_{88} - \nu_{86}$ after averaging over measured modes with degree $5 \leq l \leq 60$. The observed variation in the frequency shift can be compared with the results of the present paper in Fig. 16 and 21, where the frequency shifts, $\nu(B_p) - \nu(B$=0), are shown as functions of B_p. In our case, the spherical degree related to the maximum of the frequency shift for the p_3-mode is around 300, which is out of the interval in Libbrecht & Woodard (1990). The discrepancy between our theoretical results and Libbrecht and Woodard's observational results might be due to the fact that we only allowed for a change in the strength of the magnetic field while keeping the temperature profile and the position of the magnetic canopy unchanged.

The local maxima of the frequency shift for the p_1- and p_2-modes (Fig. 16 and 21) are likely to come from the fact that near those frequencies, the modes avoid crossings with the a-mode (see Fig. 2, 15 and 17). We argued that the a-mode is analogue to the Lamb mode, which is a global eigenmode for several model atmospheres. It propagates horizontally and is evanescent in the vertical direction. Its frequency is near the sound frequency.

In the domain of low spherical degree the effect of the magnetic field is a frequency shift of order of nHz or pHz, which is very small. For larger l, where the planar geometry can be applied, the frequency shifts are of the order of μHz, in agreement with observations.

The interaction between modes in the slow continuum is more complex than that above the slow continuum. Beside shifts in frequencies and becoming quasimodes, extra modes can ap-

pear and modes can disappear with increasing spherical degree or strength of the magnetic field. The analysis of the spatial solutions of the perturbations shows that considerable difference between the single modes in a family of split quasimodes appears only around the resonant position. The oscillation behaviour of these modes seems practically the same in the non-dissipative region. Single modes in the family of split f- and p-modes can merge for increasing magnetic field strength or wave number. There is no observational evidence of splitting of single eigenmodes into a number of quasimodes or their merge in the frequency spectrum of the solar oscillations either.

In order to obtain a more realistic picture of the global solar oscillation modes, it seems to be straightforward to change the magnetic profile in the transition layer (to avoid the jump of the magnetic field strength) and in the corona (to assume more slowly increasing or constant magnetic profile).

Global modes with wave vector parallel to the magnetic field lines can couple resonantly only to the local slow oscillations. It is of interest to examine the eigenmodes, which propagate obliquely to the magnetic field lines, and couple both to the slow modes and to the Alfvén modes. This is the field of the second part of the present analysis.

Acknowledgements. We would like to thank Petra Vanlommel for her useful comments and help to improve the manuscript. B. Pintér acknowledges the financial support obtained from the Onderzoekfounds K. U. Leuven, Belgium.

References

Abramovitz M., Stegun I., 1965, Handbook of Mathematical Functions. Dover, New York
Campbell W.R., Roberts B., 1989, ApJ 338, 538
Chen C.J., Lykoudis P.S., 1972, Solar Physics 25, 380
Christensen-Dalsgaard J., 1994, Lecture Notes on Stellar Oscillations. p. 59
Evans P., Roberts B., 1990, ApJ 356, 704
Hasan S.S., Christensen-Dalsgaard J., 1992, ApJ 396, 311
Hindman B.W., Zweibel E.G., 1994, ApJ 436, 929
Jain R., Roberts B., 1994, A&A 286, 243
Lamb H., 1932, Hydrodynamics. Cambridge University Press
Libbrecht K.G., Woodard M.F., 1990, Nat 345, 779
Tirry W.J., Goossens M., 1996, ApJ 471, 501
Tirry W.J., Goossens M., Pintér B., Čadež V.M., Vanlommel P., 1998, ApJ 503, 422
Vanlommel P., Čadeˇ z V.M., 1998, Solar Physics 182, 263